Temperature dependence of the Mn incorporation model on reconstructed P-rich GaP(001)

2008 J. Phys.: Condens. Matter 20 015006

(http://iopscience.iop.org/0953-8984/20/1/015006)

J. Phys.: Condens. Matter **20** (2008) 015006 (5pp) doi:10.1088/0953-8984/20/01/015006

Temperature dependence of the Mn incorporation model on reconstructed P-rich GaP(001)

Shiqiang Hao[1]

Department of Physics and Astronomy, The University of Tennessee, Knoxville, TN 37996, USA

Received 10 October 2007, in final form 19 November 2007
Published 7 December 2007
Online at stacks.iop.org/JPhysCM/20/015006

Abstract

Based on first-principles calculations within density functional theory and kinetic Monte Carlo simulations, kinetic pathways for Mn incorporation on a reconstructed P-rich $(2 \times 1)/(2 \times 2)$ GaP(001) growth front are proposed. During epitaxial growth, at low temperature (∼500 K) Mn dopants preserve a similar model of 'subsurface segregation' with preference for interstitial sites located below the P-dimer. At relatively high temperatures (∼900 K), Mn atoms proceed in a substitution model, characterized by the substitution of trench Ga atoms. Moreover, calculated scanning tunneling microscope images are also presented to help resolve typical surface configurations.

(Some figures in this article are in colour only in the electronic version)

1. Introduction

Heterostructure materials grown from III–V compound by precisely controlled non-equilibrium growth techniques such as molecular beam epitaxy have recently been used in numerous applications in semiconductor devices. By controlling growth conditions, the spontaneous formation of nanostructures in heteroepitaxy with unusual electronic or optical properties could be realized and even be used in high-frequency computational devices. These developments have stirred the desire to understand and even possibly control growth on an atomic scale. A wealth of conceptual advances in non-equilibrium growth have been proposed. Some especially striking works include 'surfactant action' [1] in heteroepitaxy processes and recent 'subsurface segregation' [2] in the epitaxial growth of Mn on Ge(100). Interestingly, the 'subsurface segregation' of low doses of Mn on Ge(100) are characterized by accessible interstitial sites below the Ge-dimer and are even preserved to float toward these subsurface sites during epitaxial growth of additional host Ge capping layers [2]. The findings suggest that proper *in situ* annealing after growth should alter the relative populations of the Mn in substitutional and interstitial sites and thus may cause a variation of the magnetic ordering temperature [2].

[1] Present address: Department of Chemical Engineering, Carnegie Mellon University, Pittsburgh, PA 15213, USA.

The fundamental understanding of non-equilibrium growth mechanisms has in turn impacted on the studies of fascinating properties of novel materials. Since the discovery of ferromagnetism in diluted magnetic semiconductors (DMS), such as Mn-doped GaAs or InAs, it has been intensively studied in order to establish new semiconductor spin electronics (spintronics) as a practical technology based on such new functional materials [3, 4]. As a candidate material for room temperature spintronic devices, wide band-gap DMS $Ga_{1-x}Mn_xP$ has received considerable attention [5]. For example, ferromagnetic exchange interaction in $Ga_{1-x}Mn_xP$ has been found to be mediated by holes localized in an Mn-derived band which is detached from the valence band [6]. Therefore, ferromagnetic ordering of $Ga_{1-x}Mn_xP$, together with wide band-gap nature and a property lattice-matched to Si, offer a better opportunity for integrating magnetism with existing silicon technology. On the other hand, theoretical studies [7, 8] provide the necessary knowledge of the microscopic behavior. For further understanding of the microscopic mechanism of ferromagnetic ordering in $Ga_{1-x}Mn_xP$, a detailed knowledge of spatial distribution and kinetic properties of the magnetic Mn dopants is essential. In order to study the incorporation of dopants under non-equilibrium conditions, one must identify various preferred diffusion pathways and corresponding activation barriers.

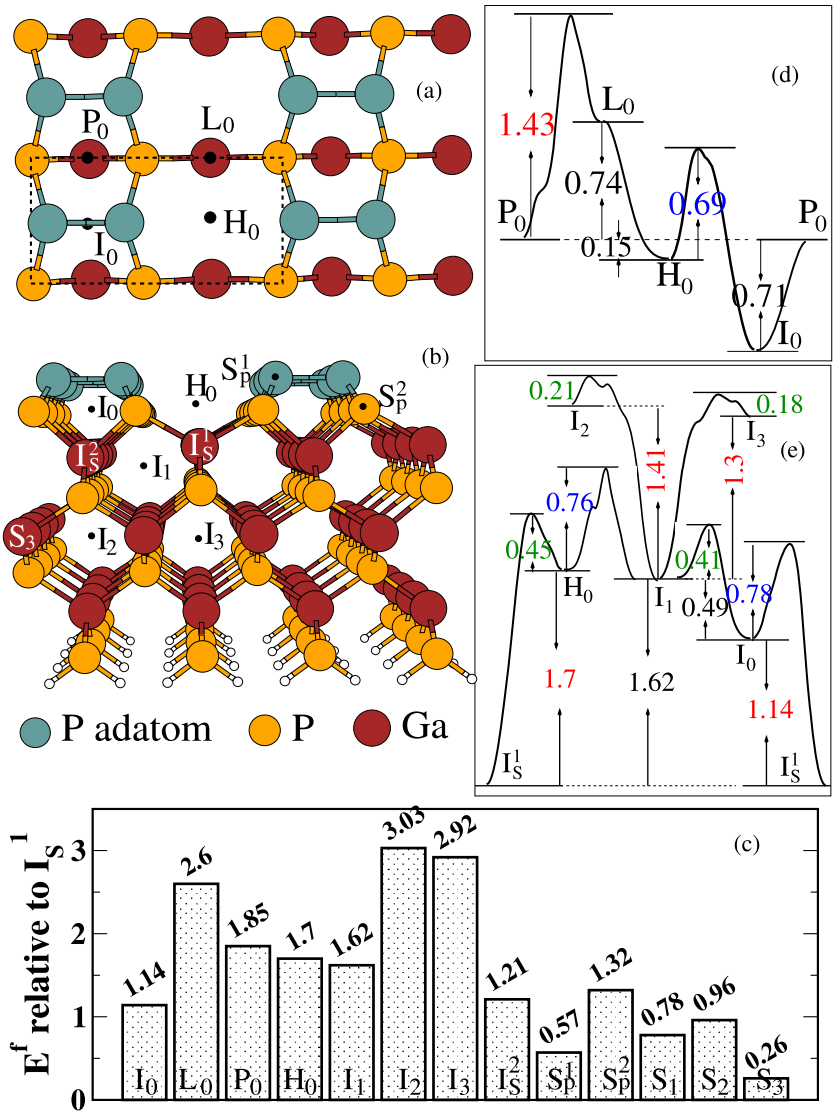

Figure 1. (a) Top view of a reconstructed $(2 \times 1)/(2 \times 2)$ GaP(001) surface with high symmetry adsorption sites, (b) side view of the surface with different interstitial and substitutional sites, (c) the formation energy relative to the most favorable I_S^1 configuration, the diffusion barriers relative to (d) I_0 and (e) I_S^1 sites. All values are in eV.

In this work, we focus our attention on the energetic and kinetic properties of Mn dopants at the growth front of GaP along the typical (001) orientation, which appears to be $(2 \times 1)/(2 \times 2)$ reconstructed by the terminating P adatoms under a wide range of P-rich conditions [9–11]. Findings from our first-principles calculations of the formation energy, minimum energy paths, and energy barriers for Mn dopants hopefully serve as important inputs in formulating a microscopic picture for the incorporation and growth of Mn on GaP.

2. Calculation methods

In this work, we use spin-polarized density functional theory (DFT) within the generalized gradient approximation [12], periodic boundary conditions, and the plane wave basis set as implemented in the Vienna *ab initio* simulation package (VASP) [13] to obtain the relaxed atomic geometries as well as their total energies. Bulk structural optimization of pure zincblende GaP results in a lattice constant of 5.503 Å, which is in good agreement with the experimental value of 5.446 Å [14]. All the surface calculations are based on an eight-layer 160-atom slab of reconstructed zincblende 4×2 GaP(001) with 13 Å vacuum as the spacing layer in the growth direction. The bottom P atoms are routinely passivated by H atoms. The projector augmented wave potentials [15, 16] have been used for all species, where 3d states of Ga and 3p states of Mn are treated as valence states. A cutoff energy of 460 eV for the plane wave basis set is adopted. A single Γ k-point sampling for this cubic lattice has been used in the Brillouin zone. The nudged elastic band method [17] is applied for finding energy barriers. All the atomic positions except the bottom Ga–P bi-layer are relaxed until the forces exerted on atoms are less than 0.03 eV Å^{-1}.

In our calculations, one Mn atom may lie in different sites within the surface region, as shown in figures 1(a) and (b). To

evaluate the relative stabilities of the various configurations, we calculate formation energies [18] of interstitial and substitutional Mn by equations (1) and (2), respectively,

$$E_{\mathrm{i}}^{f} = (E_{\mathrm{tot}}^{\mathrm{def}} - E_{\mathrm{slab}}^{\mathrm{ref}} - \mu_{\mathrm{Mn}}) \quad (1)$$

$$E_{\mathrm{s}}^{f} = (E_{\mathrm{tot}}^{\mathrm{def}} - E_{\mathrm{slab}}^{\mathrm{ref}} - \mu_{\mathrm{Mn}} + \mu_{\mathrm{X}}) \quad (2)$$

where $E_{\mathrm{tot}}^{\mathrm{def}}$ denotes the total energy of the supercell with an Mn atom, $E_{\mathrm{slab}}^{\mathrm{ref}}$ is the total energy of the slab without Mn adsorption as the reference system, and μ_{Mn} is the chemical potential of an Mn atom. For substitutional Mn adsorption or doping, the chemical potential μ_{X} depends on the substituted species. In the case of substitution of a Ga atom, the μ_{X} would be μ_{Ga}, which is calculated by $\mu_{\mathrm{Ga}} = E_{\mathrm{GaP}} - E_{\mathrm{P}}$, where the E_{GaP} and E_{P} are the total energies per formula unit of bulk zincblende GaP and bulk black phosphorus, respectively. Obviously, in the case of substitution of a P atom, the μ_{X} would be μ_{P}, which is directly found from the total energy per formula unit of bulk P. In such a way, the obtained μ_{X} vales correspond to P-rich conditions, at which the GaP(001) surface would be forming a $(2 \times 1)/(2 \times 2)$ reconstructed pattern as mentioned above.

The kinetic properties of Mn dopants can be examined numerically using kinetic Monte Carlo (KMC) simulations. The following algorithm is adopted to follow the incorporation of non-interacting Mn atoms on the GaP(001) substrate. We use a simulation unit containing 400×200 cells (a surface area of 1556×1556 Å^2) with a 0.002 coverage of randomly deposited Mn dopants on the surface as an initial configuration to measure the distribution of Mn atoms at a specific temperature. Here, the single cell is depicted as the dashed frame shown in figure 1(a) and simply assumed to be doped at most by one Mn atom, thus 0.002 coverage in 400×200 cells will give 160 Mn atoms. The layer evolution time is determined by the deposition rate, in our case, the host atoms Ga and P together with Mn dopants are deposited in a rate of one monolayer per second. At each step in our KMC algorithm, a hopping event is accepted with probability r_i/R, where r_i is the ith hopping rate and the total rate R is calculated by summing up the rates of all related hopping processes. Using transition state theory, a particular jumping rate r_i is determined by the standard Arrhenius expression $r_i = r_0 \exp(-E_{\mathrm{a}}/k_{\mathrm{B}}T)$, where the pre-exponential factor r_0 is simply adopted to be 10^{13} Hz, and E_{a} denotes the ith jumping barrier. Note that Mn cluster effects are not included in our simulations since we are interested in dilute Mn concentrations.

3. Results

Based on equations (1) and (2), the relative stabilities of various configurations as shown in figures 1(a) and (b) are investigated. We find that the energetically most favorable configuration, denoted as I_{S}^{1}, contains an Mn–Ga pair, where the Mn atom just resides in the original trench Ga site and the pushed out Ga atom has moved in a concerted manner out of the surface as a dangling neighbor to a reconstructed P adatoms. (The detailed configuration of this I_{S}^{1} is also shown in figure 2(c).) The formation energies of other configurations relative to the I_{S}^{1} site are sketched in figure 1(c). The substitutional cases, such as the substitutions of the first and second layers of Ga atoms (S_1, S_2, and S_3), adatom P (S_{p}^{1}) and surface P (S_{p}^{2}), are found to be all unfavorable. For the deeper octahedral interstitial sites, I_1, I_2, and I_3, the formation energies are much higher than those of I_{S}^{1}. It is worth mentioning that a relatively favorable surface adsorption site for an Mn adatom is the interstitial site, I_0, located 1.1 Å beneath the P-dimer (cf figure 1(a)). The other local surface adsorption sites are: a hollow site H_0 (between two trench Ga atoms), a pedestal site P_0 (on top of the non-trench Ga), and a bridge site L_0 (on top of the trench Ga). The formation energies of those metastable adsorption configurations are higher than that of I_0 by at least 0.56 eV.

Having established the preferred formation site, we now perform systemically studies on the barriers related to the hopping processes of Mn. Figure 1(d) suggests that the subsurface interstitial I_0 is actually also an accessible site, given that a hop of $H_0 \rightarrow I_0$ will encounter a relative low energy barrier of about 0.69 eV. Once in the I_0 site, there is a much smaller probability of hopping to any other surface sites (H_0, P_0, and L_0) since the corresponding barriers are much higher. As summarized in figure 1(e), the vertical pathway I_2 (or I_3) $\rightarrow I_1 \rightarrow I_0 \rightarrow I_{\mathrm{S}}^{1}$ involves a highest barrier of 0.78 eV at $I_0 \rightarrow I_{\mathrm{S}}^{1}$, and another way I_2 (or I_3) $\rightarrow I_1 \rightarrow H_0 \rightarrow I_{\mathrm{S}}^{1}$ involves a highest barrier of 0.76 eV at $I_1 \rightarrow H_0$. Based on the above results, a rough estimation would suggest that the Mn atoms would be trapped in the most favorable I_{S}^{1} site once they reach there. If they are initially in other positions, the majority of Mn atoms will keep floating with the growth process along the interstitial pathway, such as I_2 (or I_3) $\rightarrow I_1 \rightarrow I_0$ given that the growth temperature is not high enough to overcome the threshold barrier of 0.78 eV to reach the I_{S}^{1} site. On the contrary, the population of Mn atoms at the substitution site I_{S}^{1} will increase with temperature, since the probability of overcoming the threshold barrier increases.

With the knowledge of the diffusion barriers, a series of kinetic Monte Carlo (KMC) simulations can be carried out to statistically investigate the Mn distribution with growth temperature. It is found that the population of I_{S}^{1} configuration per monolayer increases by about 45% from 500 to 900 K. In other words, at low temperature, 500 K, roughly 55% Mn atoms are floating along interstitial sites, while at relatively high temperature, 900 K, almost 90% Mn atoms reside in the substitution sites I_{S}^{1}. Therefore, at relatively low temperature, Mn atoms preserve the 'subsurface segregation' during the growth of additional host atom capping layers and the subsurface I_0 sites are enriched in Mn at the initial growth stage. While at relatively high temperature, it can be deduced that the Mn atoms will keep a substitution growth, forming intrinsic $Ga_{1-x}Mn_xP$ with a very small portion ($\sim$10%) of Mn at the subsurface region. Even though the magnetism of GaMnP has been observed at room temperature [19], to the best of our knowledge, there have been no experimental results evidently indicating the Mn distribution in the GaP system.

According to the Tersoff–Hamann first-order perturbation theory [20], the tunneling current between the sample and the tip is proportional to the local electron density of states,

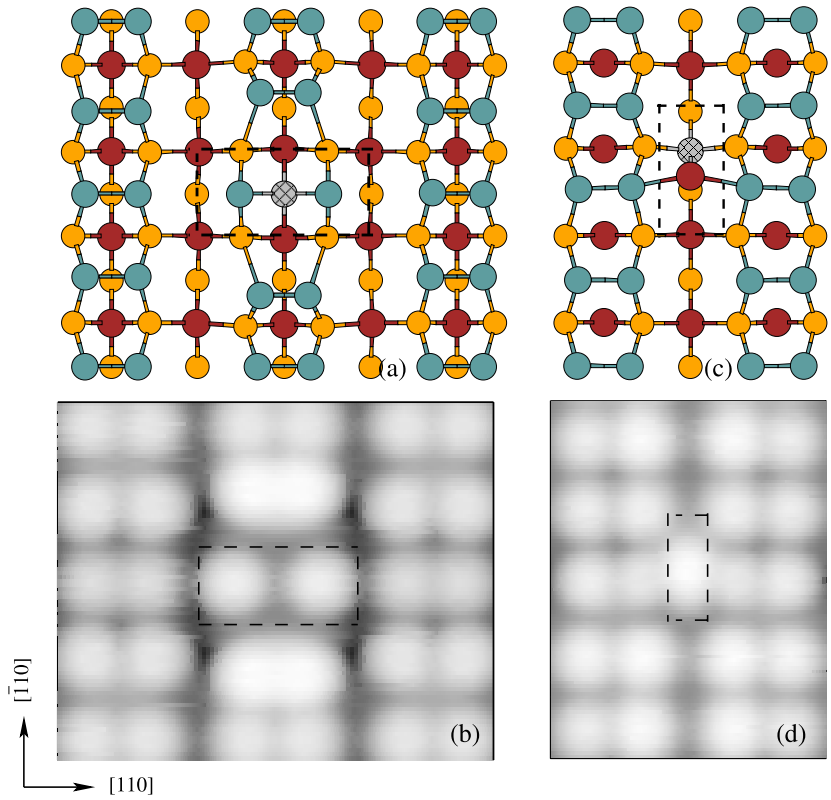

Figure 2. Top view of (a) I_0, (c) I_S^1 and corresponding calculated STM filled state images (b), (d) with bias voltage of -1.0 V, respectively. The dashed frames display the corresponding regions. The gray balls with mesh pattern are Mn, the other atoms are the same as sketched in figure 1.

meaning that scanning tunneling microscope (STM) images can be simulated. For the typical Mn configurations I_0 and I_S^1, calculated STM images are plotted. As can be seen in figure 2(b), the 'dumbbell' in the dashed frame is a characterization of I_0 with Mn beneath the broken P-dimer. The bridge between two dimer rows produced by substituting trenched Ga by Mn forming I_S^1 is also illustrated in figure 2(d) to help resolve the surface configuration.

4. Discussion and conclusion

It is interesting to note that KMC simulations at higher temperature (>900 K) have not been conducted, since the reconstructed phosphorus atoms are preferentially desorbed from the GaP surface and a well-ordered Ga-terminated surface might be formed [10], which is beyond the scope of this work. Similarly to the molecular beam epitaxy of GaAs(001) [21], due to the complexity of the surface reconstruction of GaP(001), it is normally required to consider many other processes to obtain an appropriate picture of growth. For example, some necessary processes related to host atoms would include reactions of Ga with the reconstructed P dimers, thereby splitting the dimer bond, attachment and detachment of Ga at island edges, and adsorption and desorption of P_2, etc. Therefore, our DFT calculations and KMC simulations only focus on the kinetic properties of low concentration Mn dopants on the GaP(001) front without considering more complicated processes such as nucleation of islands, diffusion along island edges and even island mobility and ripening. Moreover, the much more complex Mn–Mn clustering effects are not accounted for, since complicated processes will occur at high Mn concentration. Thus, at low temperature our model can only be applied to the initial growth stage, because at later growth stages the Mn–Mn interactions among the subsurface enriched Mn atoms and deposited Mn atoms will play more and more important roles.

KMC simulations, coupled with kinetic barriers determined by DFT, represent a powerful class of multiscale simulation approaches [21]. In our case, we should clarify that the total energies from DFT refer to absolute zero temperature, at which the $Ga_{1-x}Mn_xP$ system would be ferromagnetic. On the other hand, the system would be non-ferromagnetic at KMC simulation temperatures (500–900 K), since they are surely above the Curie temperature. Even though the total energies might be slightly different for the same configuration with different magnetic alignment states corresponding to different temperatures, the DFT barriers (refer to $T = 0$ K) from the energy difference between initial and transition states would change very little for high temperatures. For the $Ga_{1-x}Mn_xP$ system, there are not so many first-principles works addressing formation energy differences induced by spin alignments, however, from recent $Ga_{1-x}Cr_xN$ systems [22], the formation energy difference for different magnetic states with very high Mn concentration (∼3–6%) would be in a range of 10–200 meV. Thus the barrier changes would be much smaller than this, because the energies of transition states also change correspondingly. In particular, in our large supercell with dilute Mn con-

centration, the error derived from applying DFT barriers to high temperature KMC simulations is too small to affect the final statistical results.

In summary, we have carried out systematic first-principles total energy calculations and KMC simulations of the energetic and kinetic properties of Mn dopants at the reconstructed GaP(001) growth front. We find that the incorporation model of Mn dopants on reconstructed GaP(001) strongly depends on the growth temperature. At relatively low temperature, Mn atoms preserve a kind of 'subsurface segregation' during the initial stage of epitaxial growth of additional host atom capping layers to float toward the subsurface sites; while at high temperature, the majority of Mn atoms proceed in a substitution growth model, characterized by substitution of trench Ga atoms. We have also obtained the corresponding STM images of the different types of Mn configurations, which could be verified in future experiments. The main findings are intriguing not only from the point of view of fundamental growth science but also from improved understanding of the system as a DMS.

Acknowledgments

We thank Professor Zhenyu Zhang for stimulating discussions. This work was supported in part by NSF (grant no. DMR-0606485), and by DOE (CMSN grant no. DE-FG02-05ER46209, and the Division of Materials Sciences and Engineering, Office of Basic Energy Sciences, DOE, under contract DE-AC05-000R22725 with ORNL, managed by UT-Battelle, LLC). The calculations were performed at ORNL's Center for Computational Sciences.

References

[1] Copel M, Reuter M C, Kaxiras E and Tromp R M 1989 *Phys. Rev. Lett.* **63** 632
[2] Zhu W, Weitering H H, Wang E G, Kaxiras E and Zhang Z 2004 *Phys. Rev. Lett.* **93** 126102
[3] Ohno H 1998 *Science* **281** 951
[4] Ohno Y *et al* 1999 *Nature* **402** 790
[5] MacDonald A H, Schiffer P and Samarth N 2005 *Nat. Mater.* **4** 195
[6] Scarpulla M A *et al* 2005 *Phys. Rev. Lett.* **95** 207204
[7] Kronik L, Jain M and Chelikowsky J R 2004 *Appl. Phys. Lett.* **85** 2014
[8] Krstajić P M, Peeters F M, Ivanov V A, Fleurov V and Kikoin K 2004 *Phys. Rev.* B **70** 195215
[9] Pulci O, Schmidt W G and Bechstedt F 2001 *Phys. Status Solidi* a **184** 105
[10] Töben L *et al* 2001 *Surf. Sci.* **494** L755
[11] Kadotani N, Shimomura M and Fukuda Y 2004 *Phys. Rev.* B **70** 165323
[12] Perdew J P and Wang Y 1992 *Phys. Rev.* B **45** 13244
[13] Kresse G and Hafner J 1993 *Phys. Rev.* B **47** 558
[14] Villars P 1997 *Pearson's Handbook, Crystallographic Data for Intermetallic Phases* vol 2 (Materials Park, OH: ASM International) p 1903
[15] Blöchl P E 1994 *Phys. Rev.* B **50** 17953
[16] Kresse G and Joubert D 1999 *Phys. Rev.* B **59** 1758
[17] Henkelman G, Uberuaga B P and Jónsson H 2000 *J. Chem. Phys.* **113** 9901
[18] Hao S, Delley B, Veprek S and Stampfl C 2006 *Phys. Rev. Lett.* **97** 086102
Hao S, Delley B and Stampfl C 2006 *Phys. Rev.* B **74** 035424
[19] Overberg M E *et al* 2002 *J. Vac. Sci. Technol.* B **20** 969
[20] Tersoff J and Hamann D R 1983 *Phys. Rev. Lett.* **50** 1998
[21] Kratzer P and Scheffler M 2002 *Phys. Rev. Lett.* **88** 36102
[22] Cui X Y *et al* 2005 *Phys. Rev. Lett.* **95** 256404